Synthesis, structural characterization and thermal properties of Ca and La doped soda-lime glasses by laser melting

Sharafat Ali[1*], Natalia A. Wójcik[1,2], Bo Jonson[1], E. I. Kamitsos[3], Xinghua Li[4], Jian Luo[4], and Doris Möncke[1,3,5]

[1] *Department of Built Environment and Energy Technology, Linnaeus University, 35195 Växjö, Sweden*
[2] *Department of Solid State Physics, Faculty of Applied Physics and Mathematics, Gdańsk University of Technology, Narutowicza Street 11/12, 80–233 Gdańsk, Poland*
[3] *Theoretical and Physical Chemistry Institute, National Hellenic Research Foundation, 48 Vassileos Constantinou Avenue, 11635 Athens, Greece*
[4] *Glass Science and Technology, Corning Incorporated NY, USA*
[5] *Inamori School of Engineering at the New York State College of Ceramics, Alfred University, Alfred NY 14802, USA*

**corresponding author:* sharafat.ali@lnu.se

Abstract

Laser melting techniques have been used in the preparation of unconventional glass compositions with high melting temperatures. Thus, we wanted to test the feasibility of using a CO_2 laser in the preparation of nitrogen rich oxynitride glasses and nitride silicate glasses. Melting from oxides and metallic raw materials, we wanted to study first glass formation and possible evaporation losses of the glass components. Two glass series were prepared and studied for their structure and thermal properties, one with Ca^{2+}- and a higher melting La^{3+}-doped soda lime silicate series. In less than three minutes of laser melting, spheres of up to six mm diameter were successfully fabricated. The obtained glass samples were homogeneous and transparent in the visible region. X-ray diffraction and Raman spectroscopic analysis confirmed the amorphous nature of the synthesized samples. Sodium losses increase as calcium is added to the soda lime silicate glass. As expected, increasing Ca^{2+} or La^{3+} addition leady to increased depolymerization of the silicate network. Moreover, the increases in T_g with the addition of Ca^{2+} or La^{3+} ions indicating strengthening of the soda lime silicate glass by increasing strength of the M-O bonds of divalent and trivalent ions over monovalent sodium ions, weak Na-O bonds also resulting in significant evaporation loss during the short

laser melting times. The thermal stability decreases upon addition of Ca^{2+} or La^{3+} ions to the soda lime silicate glasses.

1. Introduction

Soda lime silicate glass (SLS) is one of the most important, though by non-glass scientists perhaps underappreciated, high-performance material used in scientific research, industry, and society. SLS glasses are commercially used for various products such as display and cover glasses, facades, windows, packaging, insulating materials or even bioactive materials. The key properties of these cost-efficient glasses, which makes them interesting materials, include high transparency in the visible region, high strength, high stability against crystallization, chemical durability, fiber drawing capability, compositional control of properties such as the index of refraction or coefficient of thermal expansion. Most of these properties depend on the materials structure, which varies with composition and processing conditions [1-4]. SLS glasses also have a relatively low price as compared to many other materials.

In the current paper, we prepared SLS glasses, with the additional incorporation of modifiers such as Ca^{2+} or La^{3+}, using laser melting. Laser melting is commonly used in the experimental preparation of glasses with high melting temperatures, or glasses which crystallize easily. Containerless melting and fast cooling rates can overcome crystallization, which might be observed when melting conventionally. While SLS glasses do not require laser melting, modifications, such as nitrification will increase the melting temperatures significantly. In order to better understand evaporation processes and if melting from reduced or metallic raw materials - CaH_2 and metallic lanthanum were used in this study – we employed laser melting of two SLS glass series with varying calcium and lanthanum levels. The effects of the addition either ion on the glass structure were investigated by infrared (IR) and Raman spectroscopy, while the thermal properties of the samples were studied by DTA.

Calcium and Lanthanum were selected since both ions are common network modifier ions in both oxide and oxynitride glass systems. Increasing the Ca^{2+} and/or La^{3+} ion concentration for an otherwise unchanged glass composition, leads typically to the depolymerization of the silicate network by converting bridging oxygen (BO) atoms into non-bridging oxygen (NBO) ions. However, addition of only Ca ions to the silicate glass network might induce phase separation or partial crystallization, which can degrade their mechanical and optical properties [5-8]. SLS glasses containing rare earth cations such as La^{3+}, Pr^{3+} and Er^{3+} ions have major technological applications such as laser materials, optical amplifiers in telecommunication, high-refractory lenses and other optical components [9-10]. Due to its lower cost as compared to other rare earth oxides, lanthanum is considered is an important additive in the glass industry. When La^{3+} ions are added to SLS glasses, their thermal expansion coefficient, molar volume, and electrical conductivity decrease, whereas the corrosion resistance, glass transition temperature, density, refractive index, hardness and elastic modulus increase [3, 11]. Furthermore, La^{3+} containing glasses have been proposed also as candidates for storage-matrices of radioactive waste [12]. The distribution and local environment of the of Ca^{2+} / La^{3} ions in SLS glasses lead to changes in chemical, electrical and optical properties. Therefore, it is important to understand the structural role of calcium/ lanthanum ions in the silicate glasses [13-14]. It is well known that lanthanum oxide acts as network modifier, but the local structural parameters of the La^{3+} sites in oxide glasses, as well as the distribution of coordination numbers and the assessment of La-La clusters with the existence of 'free oxide' ions that are part of the La-rich domains are still not clear [15-16]. For example, both Wilding et al. [17] and Angeli et al. [18] could not find any direct evidence for the formation of La-La clusters in silicate and borosilicate glasses, respectively. As will be shown, no evidence of La-la clusters could be found in the current investigation either.

The batch material piled on a silica substrate was melted by infrared laser energy in melting times of less than 3 minutes. The melts were always surrounded by un-melted batch material, thus, no contamination such as often introduced by the crucible material could occur.

2. Experimental

Batch compositions of $15Na_2O$-10CaO-$75SiO_2$ (in mol%) were doped with various amounts of Ca/La compounds. As noted above, CaH_2 was used as a source of Ca and metallic lanthanum as the source of La. All precursor chemicals were purchased from ChemPure (99.99% purity). 20 grams of powder in total were placed on thick silica substrate and melted by a CO_2 laser. The laser power was ramped to a power density of approximately 3 W/mm^2 in under 3 minutes. The weight of CaH_2 or La metal to SLS powder was varied from 0.5 to 2.5 wt% with increasing steps of 0.5 wt%. For each of the 10 compositions, 5 beads were prepared in each system. The melts were cooled by turning off the laser.

All samples were investigated by powder X-ray diffraction, using a Panalytical X'pert PRO MPD diffractometer and CuKα1 radiation. Powdered samples were dispersed on zero-background Si plates, and patterns were recorded using variable slits in the 2θ-range 10° – 70° for a total time of 30 min. All the samples were amorphous in nature. The homogeneity of the glasses was examined by scanning electron microscope (SEM) in backscatter mode using a LEO Gemini 1550, Zeiss, microscope. The chemical composition of the glasses was checked by energy dispersive X-ray (EDX) point analysis, using LINKAN 10000 and LINK INCA systems. The SEMs were operated at an acceleration voltage of 15 kV.

Variations in the glass structure were studied by Raman and IR spectroscopy. A dispersive confocal Raman microscope (inVia Renishaw) was used to measure the Raman spectra in the range from 100 to 2000 cm^{-1} with a resolution of 2 cm^{-1}, using the 514.5 nm laser excitation

line. For fluorescing samples, other laser excitation lines were tried as well including laser lines in the visible wavelength region at 488, 633, and 785 nm. In addition, the near-IR 1064 nm excitation line of a Nd-YAG laser was used in combination with a BRUKER RFS100 FT-Raman spectrometer, but this did not result in better resolved spectra for highly fluorescing glasses. Especially the lanthanum containing glasses exhibited strong fluorescence due to rare earth ion impurities. In any case, the best Raman spectra were recorded with 514.5 nm excitation and are presented in this work.

Infrared spectra were obtained by two methods; first, a quick screening was carried out with a Hyperion IR-microscope under air in the reflectance mode, probing different spots with dimensions of 100x100μm^2 in order to check the homogeneity of the samples, which was found generally good. Samples were positioned so that the IR microscope could probe the mostly horizontal surface in the spectral range 680-4000 cm^{-1}. Each of the displayed spectra results from the average of 128 scans. Additionally, glass pellets from pressed glass powder were analyzed in the reflectance mode on a vacuum IR spectrometer (Bruker Vertex 80v), covering the range from about 50 to 7000 cm^{-1}. An average of 100 spectra in the mid infrared (500 to 7000 cm^{-1}) and of 200 scans in the far infrared range (30 to 700 cm^{-1}) was taken for further analysis. The mid and far IR spectra were merged before Kramer-Kronig transformation, which resulted in the absorption coefficient spectra [19].

Thermal properties of samples were measured using differential scanning calorimetry (DSC). Measurements were performed on powdered samples placed in Al_2O_3 crucibles, up to 1000 °C in flowing nitrogen with a NETZSCH STA 409PC instrument and a heating rate of 20 °C min^{-1}. The onset and midpoint of the endothermic drift on the DSC curve were taken as representing T_g. The exothermic processes observed in all samples were correlated with crystallization processes. The precision in the T_g and T_{exo} values was estimated to be ± 3 ºC.

3. Results and discussion

3.1. Glass formation

A total of 10 glasses, 5 in each system were synthesized in order to determine the effect of different concentrations of Ca^{2+} or La^{3+} ions addition on the glasses structure and on the thermal properties. The analyzed glass compositions are tabulated in Table 1. X-ray diffraction patterns did not reveal sharp peaks; instead broad humps were observed confirming the amorphous nature of each sample. The glasses appear to be homogeneous, bubble-free, and optically transparent in the visible range. The elemental analysis of the laser-melted glasses showed that they contain lower contents of sodium than the target composition, the loss of Na being higher in the Ca-series than in the La-series (Table 1). The loss of Na generally increased with the addition of higher amounts of Ca^{2+} or La^{3+}. Generally, the high sodium losses compared to melt quenching, might be due to higher synthesis temperatures employed by laser melting and a much higher surface to volume ratio of small beads used in laser melting. The increase of sodium loss with calcium or lanthanum addition is more puzzling but might be related to changes of the Na-O bond strength in mixed systems. Calcium was easier incorporated than lanthanum. Adding CaH_2 to the batch could increase the CaO content from 16 to 30 mol%, while only up to 2 mol% La_2O_3 could be oxidized from the metallic La-powder and incorporated into the SLS glass base.

All the glasses contain very a minute amount of ca. 0.1% Al as a trace element, which was introduced from the raw materials.

3.2. Glass structure

3.2.1. Raman spectroscopy

The Raman spectra for the Ca- and La-series are shown in Fig. 1 (a) and (b), respectively. Band positions are indicated in each figure, where the measured broad bands are typical for silicate glasses.

A strong fluorescence background is seen to develop in the Raman spectra of the La-series. The fluorescence intensity increases with increasing La-level, since the fluorescing rare earth ions were most probably introduced by the lanthanum additions. Nevertheless, variations in the Raman spectra of the La-series are similar to those observed for the Ca-series, though less pronounced.

All glasses of the Ca- and La- series show bands at about 545-595 cm^{-1}, 790 cm^{-1}, 945 cm^{-1} and 1075-1090 cm^{-1}. These bands are typical for silicate glasses and are due to the mixed bending-stretching vibration of Si–O–Si bridges (545-595 cm^{-1}), and to the symmetric stretching of $Si–O^-$ bonds in Q^2 (945 cm^{-1}) and Q^3 (1075-1090 cm^{-1}) silicate tetrahedra with two and one non-bridging oxygen atoms (O^-), respectively [20-24]. The weak band at ~790 cm^{-1} is attributed to the Si–O–Si bending modes of oxygen bridges between silicate tetrahedra. Structural variations are more distinct for the Ca-series in Fig.1a where all spectra were scaled on the highest intensity band. Clearly, increasing Ca-levels lead to an increase in the intensity of the initially weak band at 945 cm^{-1} (Q^2) relative to the dominant band at ca. 1080 cm^{-1} (Q^3). Thus, the silicate network becomes, as expected, progressively more depolymerized at higher Ca contents. This is also consistent with the decrease in intensity of the band at about 790 cm^{-1} (Si-O-Si bridges) as bridges between Q^3 units are broken to create Q^2 units, which have two instead of the three bridging oxygen linkages in Q^3 units. The ca. 550 cm^{-1} band is also highly sensitive to the network connectivity. For low Ca-levels the maximum is found at 560 cm^{-1}, a value that is typical for a network consisting predominantly of Q^3 groups [21]. A value of 630 cm^{-1} is expected for a less polymerized networks based on Q^2 units, while the fully polymerized silicate network of Q^4 units in pure SiO_2 glass gives an intense band at lower frequency around 430 cm^{-1} [25]. Therefore, the shift of the maximum from about 560 to 595 cm^{-1} in Fig. 1a is consistent with a significant increase in depolymerization of the silicate network, in agreement with the intensity changes exhibited by the 800 and 945 cm^{-1} bands. All these

spectral variations are also in line with the progressive decrease of the SiO_2 content from glass 1Ca (70.2 mol%) to 5Ca (59.7 mol%) as seen in Table 1. The feature at 459 cm^{-1} might indicate a significant number of Q^4 units, for which the corresponding stretching modes (ν(Si-O) for Q^4) are generally weak in any Raman spectra, but would cause a broadening of the main envelope and will be reflected in a shoulder around 1200 cm^{-1}. As seen in Figure 2a, the broadness of the envelop encompassing the stretching modes decreases with Ca-addition while the band of ν(Si-O) of Q^2 units at 950 cm^{-1} increases with Ca-addition, as the network depolymerizes.

Despite the fluorescence and their high background noise, the Raman spectra of glasses in the La-series show in Fig. 1b similar trends to the glasses of the Ca-series. The spectrum of the low-La-glass (1La) is similar in form and band positions to the spectrum of the low Ca-glass (1Ca). It is noted that the lower frequency of the mixed bending-stretching mode of Si–O–Si bridges at 545 cm^{-1} for glass 1La suggests a higher degree of polymerization of the silicate network than in glass 1Ca; this is consistent with the higher silica content of 1La (74.3 mol% SiO_2, Table 1). La-addition leads to a relative increase of the 950 cm^{-1} feature signifying the formation of more Q^2 silicate tetrahedra. The 545 cm^{-1} band appears to shift to about 595 cm^{-1}, indicating also increasing depolymerization of the silicates network. In line with this trend is the frequency downshift of the high-frequency band from 1090 to 1075 cm^{-1}, as the La content increases from 0.5 to 2 mol%.

3.2.2. IR spectroscopy

Absorption coefficient spectra of glasses in the Ca- and La-series are depicted in Figures 2a and 2b, respectively. The spectra show infrared activity in four distinct spectral regions. The most prominent band is centered near 1080-1095 cm^{-1} and is assigned to the asymmetric

stretching vibration of Si-O bonds in Q^3 type silicate tetrahedra (for band assignments see [20-22, 25-29] and references therein). The shoulder at about 1200 cm^{-1}, which is most pronounced in the IR spectra of the least modified glasses 1Ca and 1La and remains strong for all other La-glasses analyzed, reflects the presence of a significant population of Q^4 type tetrahedra, i.e. of fully bridged silicate tetrahedra. The shoulder at the low frequency side of the high frequency envelope, which becomes stronger with Ca-addition, signifies the formation of the less polymerized Q^2 units. The weaker band at ca. 785 cm^{-1} results from the bending modes of Si-O-Si bridges, while the rocking motion of Si-O-Si bridges gives rise to the band at 497 cm^{-1} the positon of which is sensitive to the depolymerization of the silicate network [20]. In the far-IR region, there is a broad envelope at about 265 cm^{-1} that shows a relative increase with Ca-addition (Fig.2a). This envelop should originate from the overlap of bands due to Na^+-site vibrations around 200-250 cm^{-1} and [20-22, 27] Ca^{2+}-site vibrations around 240-280 cm^{-1} [30-32] depending on glass composition. The far-IR profile remains almost constant for the La-series, with no La^{3+}-site vibration band being distinguished at ca. 190-200 cm^{-1} [30] due to the low levels of La^{3+} incorporated in the glasses of this study. Only three La-containing glasses (1La, 3La and 4La) gave enough material and were of sufficient size to be studied by IR reflectance spectroscopy. The used aperture in the far-IR was about 3 mm, which gives a measuring spot size of roughly 5 mm in diameter, averaging the signal over the whole area.

The effect of composition on the IR spectra of glasses in the Ca-series is shown in (Figs. 3 a to c, which display three spectral regions in expended frequency and/or intensity scales. The Si-O-Si rocking vibration band upshifts from 493 to 502 cm^{-1}; while the Si-O-Si bending mode losses intensity and downshifts from 784 to 771 cm^{-1} with Ca-addition. In parallel, the Si-O stretching mode of Q^3 species downshifts from 1082 to 1065 cm^{-1} and the band of Q^4 species losses relative intensity in favor of Q^2 species All these observations confirm the results obtained from Raman spectroscopy and are consistent with an increased

depolymerization of the silicate glass network with Ca addition. Like the Raman spectra, structural variations of the IR spectra are smaller for glasses in the La-series compared to those of the Ca-series (see Fig.2).

3.3 Thermal properties

The glass transition T_g, the onset T_1 and peak position T_2 temperatures of exothermic processes, and the glass stabilities S_1, S_2 were determined for all glasses samples and are listed in Table 2. The glass stability is an often-used indicator describing the resistance to crystallization during heating. It is typically expressed by the difference between the first crystallization onset value and the glass transition temperature, $S_1 = T_1 - T_g$, or the first exothermic peak position and glass transition temperatures, $S_2 = T_2 - T_g$. The thermal properties are shown as a function of the effective cation field strength (ECFS) of the modifier cations. The cation field strengths (CFSs) of the modifier ions were calculated using CFS = Z/r^2 where "Z" is the valence of the respective cation and "r" the Shannon-Prewitt ionic radius for 8-coordinated Na and La and 7-coordinated Ca, which is 0.718, 1.780, 2.229, $Å^{-2}$ for Na^+, Ca^{2+}, La^{3+}, respectively. The ECFS was calculated as for the La-series by ECFS = $x_{Na}\cdot CFS_{Na} + x_{Ca}\cdot CFS_{Ca} + x_{La}\cdot CFS_{La}$, with x_{Na}, x_{Ca} and x_{La} being the atomic fractions of Na, Ca and La, respectively. As expected within each series, the changes in ECFS follow the changes in x. The composition dependence of the of glass transition temperature (T_g) and glass stability is given in Table 2 and presented in Fig. 4a and 4b, as a function of effective cation field strength (ECFS). The T_g values increase with increasing Ca^{2+} or La^{3+} addition to the soda lime glass, despite the spectroscopic results that both Ca^{2+} and La^{3+} act as network modifiers and depolymerize the glass network. This observation emphasizes the importance of forming Ca-O and La-O bonds, which cross-link effectively the silicate network and contribute to the enhancement of the glass T_g temperature compared to other modifier cations [20, 31]. The higher

values of T_g for the La-series is due to the high cation field strength of La^{3+} compared to the lower valence Ca^{2+} or Na^{+} ions. For the Ca-series, there is the additional effect of losing up to 10-20 mol% Na_2O during synthesis by laser melting; this replacement of the monovalent Na^{+} by the stronger cross-linker Ca^{2+} overcomes the observed effect of an slightly increased degree of silicate depolymerization. An increase in T_g for both alkaline-earth and rare-earth oxide [3, 32-35] as well as oxynitride glasses [6, 36-38] but also for tellurites [39] and phosphate glasses [40-41] melted in Al_2O_3 crucibles has been observed in earlier studies. For all the cited cases, a very strong cross-linking capacity of the added modifier cations may overcome the weakening effect due to network depolymerization.

Generally, a higher value of stability implies that the glass composition is more resistant to crystallization upon heat treatment. The glass stability decreases with increasing the Ca^{2+}/La^{3+} addition as shown in Fig. 4b. These findings are consistent with the Bingham et al [42] results that the amount of modifier added to the glass network effect on the stability of glass and decreases with increasing alkaline-earth modifiers.

Conclusions

Soda-lime glasses of initial composition $15Na_2O$-$10CaO$-$75SiO_2$ (in mol%) were doped with Ca^{2+} or La^{3+} by laser melting in less than 3 minutes, even when using CaH_2 or metallic La as raw materials. The addition of Ca^{2+}/La^{3+} ions results in changes in the glass structure and thermal properties. A relative high loss (10-20%) of Na-ions was observed with the addition of CaH_2, despite the short synthesis time employed. Both IR and Raman spectra of the laser-melted glasses manifest clear signatures of significant silicate network depolymerization as the amount of Ca^{2+} or La^{3+} increases. The glass transition temperature increases with the addition of Ca or La ions, due to the strong cross-linking of the silicate network through Ca-oxygen or La-oxygen ionic bonds. However, the glass stability decreases in the same order

because of the higher tendency for crystallization of the depolymerized silicate structure. Laser melting provides access to many high melting glass compositions previously not accessible, but the loss of volatile elements, even at very short melting times can be significant.

4. Acknowledgements

SA acknowledges the financial support from the Crafoord Foundation (Grant No: 20160900, ÅForsk Foundation (Grant No. 14-457) and Vinnova (Grant No. 2015-04809). DM thanks the Knowledge Foundation (Grant No. 68110029) for financing her stay 2017/2018 at Linnæus University. EIK acknowledge the project "National Infrastructure in Nanotechnology, Advanced Materials and Micro - / Nanoelectronics" (MIS 5002772) which is implemented under the Action "Reinforcement of the Research and Innovation Infrastructure", funded by the Operational Program "Competitiveness, Entrepreneurship and Innovation" (NSRF 2014-2020) and co-financed by Greece and the European Union (European Regional Development Fund).

Reference

1. Cormier L, Calas G, Beuneu B. Structural changes between soda-lime silicate glass and melt. J Non-Cryst Solids. 2011;357(3):926-31.
2. Wondraczek L, Mauro JC, Eckert J, Kuhn U, Horbach J, Deubener J, et al. Towards Ultrastrong Glasses. Advanced Materials. 2011;23(39):4578-86.
3. Iftekhar S, Grins J, Edén M. Composition–property relationships of the La2O3–Al2O3–SiO2 glass system. J Non-Cryst Solids. 2010;356(20):1043-8.
4. Le J, Song LX, Peng XF, Hu XF. Fracture mechanics analysis of thermally tempered glass plate: fracture induced by an embedded crack. International Journal of Fracture. 2005;132(4):299-309.
5. Sebdani MM, Mauro JC, Jensen LR, Smedskjaer MM. Structure-property relations in calcium aluminate glasses containing different divalent cations and SiO2. J Non-Cryst Solids. 2015;427:160-5.
6. Sharafat A, Grins J, Esmaeilzadeh S. Glass-forming region in the Ca–Si–O–N system using CaH_2 as Ca source. J Eur Ceram Soc. 2008;28(14):2659-64.
7. Sharafat A, Grins J, Esmaeilzadeh S. Hardness and refractive index of Ca-Si-O-N glasses. J Non-Cryst Solids. 2009;355(4-5):301-4.
8. Ali S, Paul B, Magnusson R, Broitman E, Jonson B, Eklund P, et al. Synthesis and characterization of the mechanical and optical properties of Ca-Si-O-N thin films deposited by RF magnetron sputtering. Surface and Coatings Technology. 2017;315:88-94.
. Schaller T, Stebbins JF. The Structural Role of Lanthanum and Yttrium in Aluminosilicate Glasses: A 27Al and 17O MAS NMR Study. The Journal of Physical Chemistry B. 1998;102(52):10690-7.
0. Schuster K, Litzkendorf D, Grimm S, Kobelke J, Schwuchow A, Ludwig A, et al. Study of lanthanum aluminum silicate glasses for passive and active optical fibers: SPIE; 2013.

11. Mahdy EA, Ibrahim S. Influence of Y2O3 on the structure and properties of calcium magnesium aluminosilicate glasses. Journal of Molecular Structure. 2012;1027:81-6.
12. Bardez I, Caurant D, Loiseau P, Baffier N, Dussossoy JL, Gervais C, et al. Structural characterisation of rare earth rich glasses for nuclear waste immobilisation. Physics and Chemistry of Glasses. 2005;46(4):320-9.
13. Gaddam A, Fernandes HR, Tulyaganov DU, Ferreira JMF. The structural role of lanthanum oxide in silicate glasses. J Non-Cryst Solids. 2019;505:18-27.
14. Ellison AJG, Hess PC. Lanthanides in silicate glasses: A vibrational spectroscopic study. Journal of Geophysical Research: Solid Earth. 1990;95(B10):15717-26.
15. Park B, Li H, Corrales LR. Molecular dynamics simulation of La2O3–Na2O–SiO2 glasses. I. The structural role of La3+ cations. J Non-Cryst Solids. 2002;297(2):220-38.
16. Schaller T, Stebbins JF, Wilding MC. Cation clustering and formation of free oxide ions in sodium and potassium lanthanum silicate glasses: nuclear magnetic resonance and Raman spectroscopic findings. J Non-Cryst Solids. 1999;243(2):146-57.
17. Wilding M, Badyal Y, Navrotsky A. The local environment of trivalent lanthanide ions in sodium silicate glasses: A neutron diffraction study using isotopic substitution. J Non-Cryst Solids. 2007;353(52):4792-800.
18. Angeli F, Charpentier T, Molières E, Soleilhavoup A, Jollivet P, Gin S. Influence of lanthanum on borosilicate glass structure: A multinuclear MAS and MQMAS NMR investigation. J Non-Cryst Solids. 2013;376:189-98.
19. Kamitsos EI, Chryssikos GD. Borate glass structure by Raman and infrared spectroscopies. Journal of Molecular Structure. 1991;247:1-16.
20. Wójcik NA, Ali S, Möncke D, Tagiara NS, Kamitsos EI, Segawa H, et al. The influence of Be addition on the structure and thermal properties of alkali-silicate glasses. J Non-Cryst Solids. 2019;521:119532.
21. Kamitsos EI, Kapoutsis JA, Jain H, Hsieh CH. Vibrational study of the role of trivalent ions in sodium trisilicate glass. J Non-Cryst Solids. 1994;171(1):31-45.
22. Kamitsos EI, Risen WM. Vibrational spectra of single and mixed alkali pentasilicate glasses. J Non-Cryst Solids. 1984;65(2):333-54.
23. Furukawa T, Fox KE, White WB. Raman spectroscopic investigation of the structure of silicate glasses. III. Raman intensities and structural units in sodium silicate glasses. The Journal of Chemical Physics. 1981;75(7):3226-37.
4. Brawer SA, White WB. Raman spectroscopic investigation of the structure of silicate glasses. I. The binary alkali silicates. The Journal of Chemical Physics. 1975;63(6):2421-32.

25. Efthimiopoulos I, Palles D, Richter S, Hoppe U, Möncke D, Wondraczek L, et al. Femtosecond laser-induced transformations in ultra-low expansion glass: Microstructure and local density variations by vibrational spectroscopy. Journal of Applied Physics. 2018;123(23):233105.
26. Wójcik NA, Jonson B, Möncke D, Kamitsos EI, Segawa H, Karczewski J, et al. The effect of nitrogen on the structure and thermal properties of beryllium-containing Na-(Li)-Si-O-N glasses. J Non-Cryst Solids. 2019;522:119585.
27. Grund Bäck L, Ali S, Karlsson S, Möncke D, Kamitsos EI, Jonson B. Mixed alkali/alkaline earth-silicate glasses: Physical properties and structure by vibrational spectroscopy. International Journal of Applied Glass Science. 2019;10(3):349-62.
28. Dussauze M, Rodriguez V, Lipovskii A, Petrov M, Smith C, Richardson K, et al. How Does Thermal Poling Affect the Structure of Soda-Lime Glass? The Journal of Physical Chemistry C. 2010;114(29):12754-9.
29. M.D. Ingram JED, A.M. Coats, E.I. Kamitsos, J.A. Kapoutsis,. Origins of anomalous mixed-alkali effects in ion-exchanged glasses,. Glass Science and Technology-Glastechnische Berichte. 2000;73(4):89-104.
30. Nelson BN, Exarhos GJ. Vibrational spectroscopy of cation-site interactions in phosphate glasses. The Journal of Chemical Physics. 1979;71(7):2739-47.
31. Möncke D, Kamitsos EI, Palles D, Limbach R, Winterstein-Beckmann A, Honma T, et al. Transition and post-transition metal ions in borate glasses: Borate ligand speciation, cluster formation, and their effect on glass transition and mechanical properties. The Journal of Chemical Physics. 2016;145(12):124501.
32. Iftekhar S, Leonova E, Edén M. Structural characterization of lanthanum aluminosilicate glasses by 29Si solid-state NMR. J Non-Cryst Solids. 2009;355(43):2165-74.
33. Takahashi S, Neuville DR, Takebe H. Thermal properties, density and structure of percalcic and peraluminus $CaO–Al_2O_3–SiO_2$ glasses. J Non-Cryst Solids. 2015;411:5-12.
34. Stevensson B, Eden M. Structural rationalization of the microhardness trends of rare-earth aluminosilicate glasses: Interplay between the RE3+ field-strength and the aluminum coordinations. J Non-Cryst Solids. 2013;378:163-7.
35. Smedskjaer MM, Mauro JC, Kjeldsen J, Yue YZ. Microscopic Origins of Compositional Trends in Aluminosilicate Glass Properties. J Am Ceram Soc. 2013;96(5):1436-43.
36. Ali S, Jonson B. Glasses in the Ba-Si-O-N System. J Am Ceram Soc. 2011;94(9):2912-7.
7. Sharafat A, Forslund B, Grins J, Esmaeilzadeh S. Formation and properties of nitrogen-rich strontium silicon oxynitride glasses. J Mater Sci. 2009;44(2):664-70.
8. Hakeem AS, Grins J, Esmaeilzadeh S. La-Si-O-N glasses - Part I. Extension of the glass forming region. J Eur Ceram Soc. 2007;27(16):4773-81.

39. Tagiara NS, Palles D, Simandiras ED, Psycharis V, Kyritsis A, Kamitsos EI. Synthesis, thermal and structural properties of pure TeO_2 glass and zinc-tellurite glasses. J Non-Cryst Solids. 2017;457(Supplement C):116-25.

40. Konidakis I, Varsamis CPE, Kamitsos EI. Effect of synthesis method on the structure and properties of AgPO3-based glasses. J Non-Cryst Solids. 2011;357(14):2684-9.

41. Palles D, Konidakis I, Varsamis CPE, Kamitsos EI. Vibrational spectroscopic and bond valence study of structure and bonding in Al2O3-containing AgI-$AgPO_3$ glasses. RSC Advances. 2016;6(20):16697-710.

42. Bingham PA, Hand RJ, Hannant OM, Forder SD, Kilcoyne SH. Effects of modifier additions on the thermal properties, chemical durability, oxidation state and structure of iron phosphate glasses. J Non-Cryst Solids. 2009;355(28):1526-38.

Table 1. Analyzed composition for all prepared glasses

Glass ID	Analyzed Composition (wt%)	Analyzed composition (at%)	Analyzed composition (mol%)
		Series I samples	
1Ca	$Na_{10.0}Ca_{11.4}Si_{33.2}O_{45.8}$	$Na_{9.1}Ca_{6.0}Si_{24.9}O_{60.1}$	$12.9Na_2O$-16.9CaO-70.2SiO_2
2Ca	$Na_{9.7}Ca_{15.5}Si_{31.4}O_{44.5}$	$Na_{8.9}Ca_{8.2}Si_{23.8}O_{59.0}$	$11.9Na_2O$-21.8CaO-66.4SiO_2
3Ca	$Na_{8.5}Ca_{18.4}Si_{30.4}O_{44.6}$	$Na_{7.8}Ca_{9.8}Si_{23.1}O_{59.3}$	$10.7Na_2O$-26.6CaO-62.7SiO_2
4Ca	$Na_{8.2}Ca_{20.2}Si_{29.1}O_{43.9}$	$Na_{7.7}Ca_{10.9}Si_{22.5}O_{58.9}$	$10.4Na_2O$-29.3CaO-60.3SiO_2
5Ca	$Na_{7.8}Ca_{20.9}Si_{28.8}O_{43.82}$	$Na_{7.3}Ca_{11.3}Si_{22.2}O_{59.2}$	$9.9Na_2O$-30.4CaO-59.7SiO_2
		Series II samples	
1La	$Na_{11.6}Ca_{6.9}La_{2.1}Si_{35.0}O_{46.1}$	$Na_{10.5}Ca_{3.6}La_{0.3}Si_{25.9}O_{59.8}$	$15.0Na_2O$-10.3CaO-0.5La_2O_3-74.3SiO_2
2La	$Na_{10.9}Ca_{6.5}La_{4.1}Si_{33.8}O_{45.4}$	$Na_{10.1}Ca_{3.5}La_{0.6}Si_{25.6}O_{60.3}$	$14.7Na_2O$-10.0CaO-0.9La_2O_3-74.4SiO_2
3La	$Na_{09.2}Ca_{8.0}La_{7.5}Si_{31.7}O_{43.6}$	$Na_{08.9}Ca_{4.4}La_{1.2}Si_{25.1}O_{60.5}$	$12.9Na_2O$-12.8CaO-1.7La_2O_3-72.6SiO_2
4La	$Na_{10.1}Ca_{7.6}La_{8.3}Si_{31.0}O_{43.5}$	$Na_{09.7}Ca_{4.2}La_{1.31}Si_{24.5}O_{60.2}$	$14.2Na_2O$-12.3CaO-1.9La_2O_3-71.5SiO_2
5La	$Na_{09.1}Ca_{7.9}La_{8.5}Si_{30.8}O_{43.1}$	$Na_{08.8}Ca_{4.4}La_{1.4}Si_{24.7}O_{60.5}$	$13.0Na_2O$-12.9CaO-2.0La_2O_3-72.2SiO_2

Table 2. DSC results and glass stabilities for all prepared glasses

ID	ECFS (Å^{-2})	$T_{g\,onset}$ (°C)	$T_{g\,mid}$ (°C)	T_1 (°C)	T_2 (°C)	S_1 (°C)	S_2 (°C)
1Ca	1.14	621	640	881	909	260	288

2Ca	1.23	627	642	861	881	234	254
3Ca	1.30	646	659	845	869	199	223
4Ca	1.34	654	669	842	865	188	211
5Ca	1.36	672	680	819	841	147	169
1La	1.02	611	618	-	-	-	-
2La	1.05	626	630	-	-	-	-
3La	1.18	631	648	945	967	319	341
4La	1.17	639	645	927	938	290	299
5La	1.26	662	676	942	961	280	285
Error		±3	±3	±3	±3	±3	±3

Figure 1: *Normalized (without baseline correction) Raman spectra for (a) Ca-series and (b) La-series. Selected band positions are indicated in the figures. Spectra are off-set for clarity. (All spectra were measured with the 514.5 nm excitation line. For glass compositions see Table 1).*

Figure 2: *Infrared absorption spectra of glasses from the (a) Ca-series and (b) La-series. The spectra are normalized to the intensity of the strongest band (1090 cm^{-1}).*

Figure 3: *Details of the infrared absorption spectra of Figure 2 a for the Ca-series displaying (a) the far-infrared region of cation-motion bands and the Si-O-Si rocking vibration at ca. 495 cm^{-1}, magnified x2, (b) the Si-O-Si bending band, magnified x6, and (c) the Si-O stretching activity of Q^n silicate units.*

Figure 4: *Comparison of (a) Tg temperatures and (b) glass stabilities for all glasses prepared and listed in Table 2.*

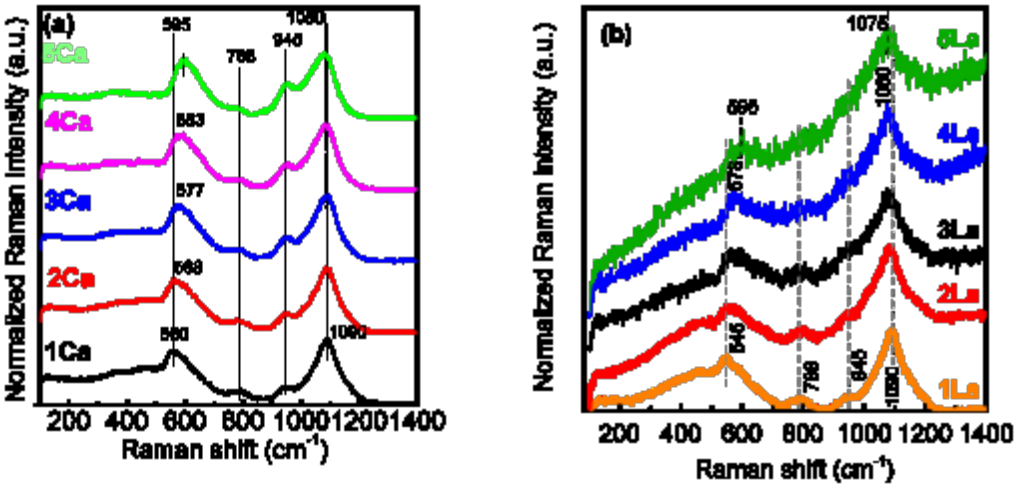

Figure 1:

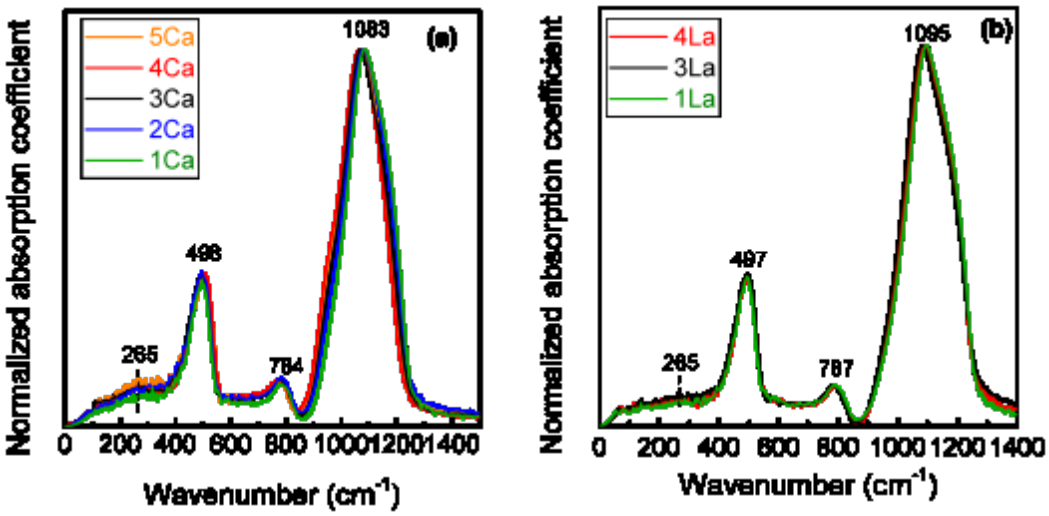

Figure 2:

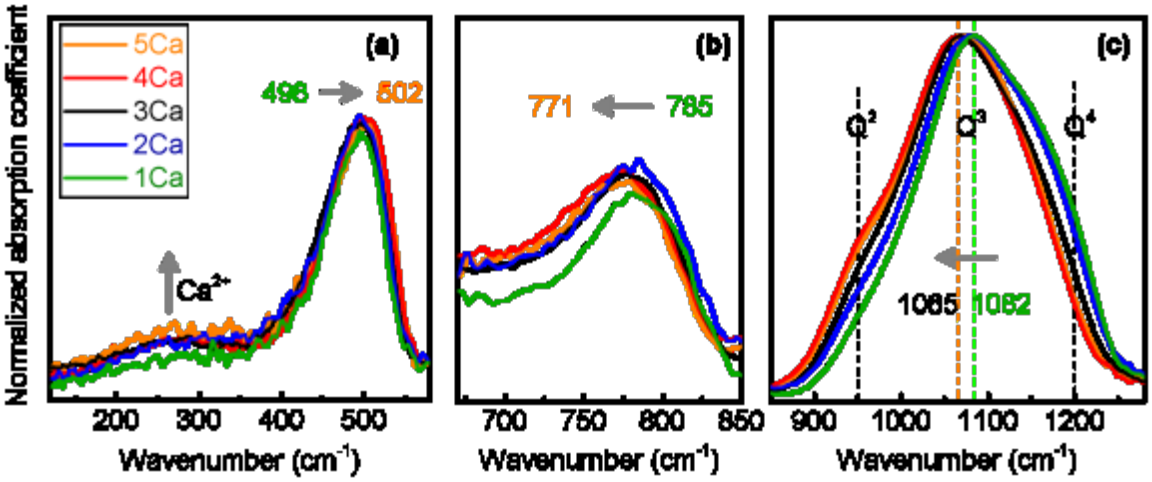

Figure 3:

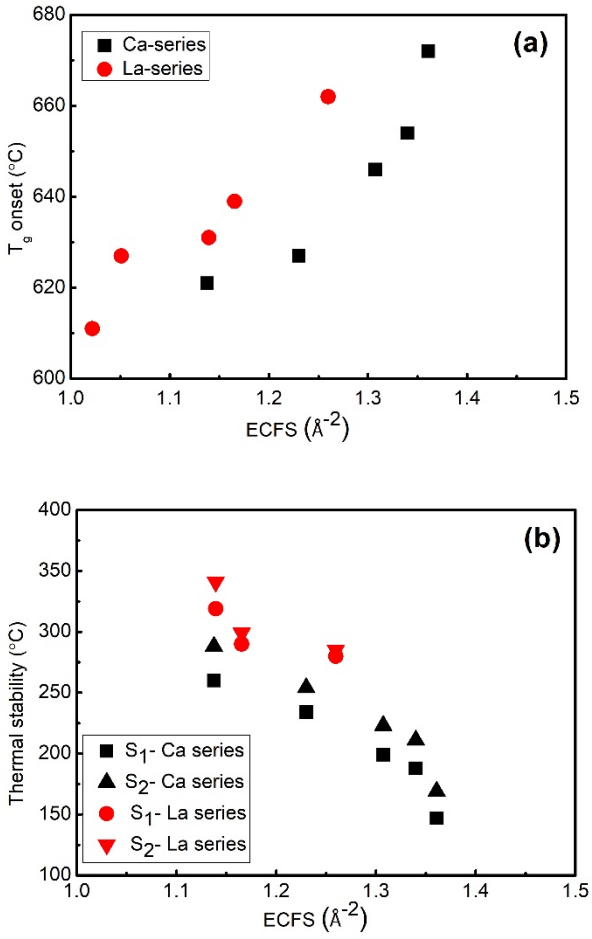

Figure 4: